Steady-State Kinetics of the Hypoxanthine-Guanine-Xanthine Phosphoribosyltransferase from *Tritrichomonas foetus*: The Role of Threonine-47[†]

Narsimha R. Munagala, Marian S. Chin, and Ching C. Wang*

Department of Pharmaceutical Chemistry, School of Pharmacy, University of California, San Francisco, California 94143-0446

Received October 10, 1997; Revised Manuscript Received January 2, 1998

ABSTRACT: *Tritrichomonas foetus*, an anaerobic flagellated protozoan, causes urogenital trichomoniasis in cattle. Hypoxanthine-guanine-xanthine phosphoribosyl transferase (HGXPRTase), an essential enzyme in *T. foetus* required for salvaging exogenous purine bases, has been regarded as a promising target for anti-tritrichomonial chemotherapy. The steady-state kinetic analyses of synthesis and pyrophosphorolysis of IMP, GMP, and XMP and product inhibition studies have been used to elucidate the reaction mechanisms. Double-reciprocal plots of initial velocities versus the varying concentrations of one substrate at a fixed concentration of the other show intersecting lines indicating a sequential mechanism for both the forward and the reverse reactions. In terms of the k_{cat}/K_m ratios, hypoxanthine is the most effective substrate whereas guanine and xanthine are converted equally well into their corresponding nucleotides. The minimum kinetic model from the data in product inhibition studies is an ordered bi−bi mechanism, where the substrates bind to the enzyme (first PRPP followed by the purine bases), and the products released (first PPi followed by purine nucleotide) in a defined order. The K_ms for PPi in the *T. foetus* HGXPRTase-catalyzed reactions are unusually high, close to the millimolar range. Since the crystal structure of this enzyme [Somoza et al. (1996) *Biochemistry 35*, 7032−7040] suggests potential binding between the threonine-47 in a conserved *cis*-peptide loop and PPi whereas human HGPRTase has lysine-68 [Eads et al. (1994) *Cell 78*, 325−334] at the corresponding position, we prepared a T47K enzyme mutant and found in the T47K-catalyzed reaction a 4−10-fold decrease of K_m for PPi. The lack of ionic interactions between Thr-47 and PPi and an increased distance between the loop and the active site as compared to the human HGPRTase are thus proposed to be responsible for the high K_m for PPi in the *T. foetus* HGXPRTase-catalyzed reaction.

Purine phosphoribosyltransferases (PRTases) form a family of enzymes that catalyze the transfer of the phosphoribosyl moiety from α-D-5-phosphoribosyl-1-pyrophosphate (PRPP)[1] to the imidazole N-9 of a purine base to form a purine nucleotide and pyrophosphate. This reaction occurs with an anomeric inversion of the ribosyl C1 from the α- to the β-conformation (*1*). These enzymes play an important role in the purine salvages among a variety of living organisms (*2*−*10*). The mechanisms of a few of the purine phosphoribosyltransferases have been studied. The human hypoxanthine-guanine phosphoribosyltransferase- (HGPRTase) (*11*) and *Schistosoma mansoni* HGPRTase-catalyzed reactions (*12*) are known to proceed with ordered binding of substrates and ordered release of products. Ordinarily, PRPP binds to the free enzyme first, followed by the binding of the purine base. After the completion of the reaction, pyrophosphate is first released and then the purine nucleotide.

Tritrichomonas foetus is an anaerobic parasitic protozoan infecting bovine uterus and is a cause of fetal abortions and sterility in cattle (*13*, *14*). This organism is incapable of performing de novo synthesis of purine nucleotides and relies primarily on its hypoxanthine-guanine-xanthine phosphoribosyltransferase (HGXPRTase) to salvage exogenous purine bases to replenish its purine nucleotide pool (*10*). This enzyme has been thus proposed as a potential target for the design of chemotherapeutic agents against this parasite (*10*, *15*, *16*). To design specific inhibitors of the parasite enzyme, detailed kinetic analyses of both the *T. foetus* HGXPRTase- and the mammalian HGPRTase-catalyzed reactions will be necessary to elucidate potential discrepancies in the catalytic properties between the two enzymes. The kinetic data on the human HGPRTase-catalyzed reactions have been already available (*11*, *17*). The cDNA encoding *T. foetus* HGXPRTase has been cloned and expressed in *Escherichia coli* to yield large quantities of purified recombinant enzyme in its native form (*16*). In the present study, hypoxanthine, guanine, and xanthine were each scrutinized and verified as similarly effective substrates of the enzyme. Product inhibition studies were conducted in both the forward and reverse reactions to elucidate the mechanism of catalysis. One main distinctive feature of the parasite enzyme is the unusually high K_m value for pyrophosphate (PPi) (165−739 μM, depending on the purine nucleotide) (Table 1) when compared with the value of 25 μM in human HGPRTase-catalyzed reaction (*11*).

[†] This work was supported by National Health Grant AI 19391.

* To whom correspondence should be addressed at the Department of Pharmaceutical Chemistry, University of California San Francisco, San Francisco, CA 94143-0446.

[1] Abbreviations: HGPRTase, hypoxanthine-guanine phosphoribosyltransferase; HGXPRTase, hypoxanthine-guanine-xanthine phosphoribosyltransferase; PRPP, 5-phosphorylribose-1-pyrophosphate; PPi, pyrophosphate.

S0006-2960(97)02515-4 CCC: $15.00
Published on Web 03/06/1998

Table 1: Kinetic Constants of the Wild-Type *T. foetus* HGXPRTase-Catalyzed Reactions

substrate	K_m (μM)	V_{max} (μmol min^{-1} mg^{-1})	k_{cat} (s^{-1})
	HPRTase		
hypoxanthine	3.05 ± 0.54	26.52 ± 1.37	8.92 ± 0.46
PRPP	39.9 ± 5.59	21.7 ± 1.75	7.57 ± 0.61
IMP	12.09 ± 0.698	0.549 ± 0.08	0.192 ± 0.03
PPi	282.91 ± 77.8	0.436 ± 0.06	0.152 ± 0.02
	GPRTase		
guanine	2.4 ± 0.74	7.1 ± 0.68	2.48 ± 0.24
PRPP	46 ± 7.2	5.45 ± 0.26	1.88 ± 0.09
GMP	23.3 ± 4.7	2.64 ± 0.2	0.92 ± 0.07
PPi	165.5 ± 43.4	2.25 ± 0.17	0.78 ± 0.06
	XPRTase		
xanthine	6.08 ± 0.81	13.93 ± 2.31	4.82 ± 0.80
PRPP	43.77 ± 3.49	12.02 ± 1.79	4.16 ± 0.62
XMP	31.46 ± 7.16	0.503 ± 0.04	0.17 ± 0.015
PPi	739.13 ± 73.11	0.640 ± 0.06	0.223 ± 0.023

The three-dimensional structure of human HGPRTase was identified by X-ray crystallography with a resolution of 2.5 Å (*18*), and the structure of *T. foetus* HGXPRTase was dissected at a resolution of 1.9 Å (*19*). There is a loop between the β-strand 3 and the α-helix 3 in the human enzyme that has been postulated to be involved in PRPP binding with K68 in the loop interacting specifically with the pyrophosphate moiety of PRPP (*18*). There is a similar loop between the β-strand 2 and the α-helix 2 in the *T. foetus* enzyme, except that the loop position corresponding to K68 in the human enzyme is replaced by T47 (*19*). To verify whether the potential lack of ionic interaction between T47 and the pyrophosphate moiety of PRPP may have precipitated the high K_m of PPi in *T. foetus* HGXPRTase, we generated the T47K mutant of the parasite enzyme by site-directed mutagenesis and found a significant decrease of the K_m value for PPi by 4−10-fold without any appreciable change in the k_{cat} values and the K_m for PRPP.

MATERIALS AND METHODS

Materials. All reagents, including hypoxanthine, guanine, xanthine, IMP, GMP, XMP, PPi, and the tetrasodium salt of PRPP, were purchased from Sigma Chemical Co. (St. Louis, MO) and of the highest purity available. Xanthine oxidase (1 unit/mg of protein) was from Boehringer Mannheim (Indianapolis, IN), and the guanase (0.1 unit/mg of protein) was from Sigma Chemical Co. (St. Louis, MO).

Enzyme Purification. The recombinant *T. foetus* HGXPRTase wild-type and T47K mutant were each purified to homogeneity from low-phosphate-induced *E. coli* SØ606 transformed with the pBTfprt expression plasmid (*16*) as described by Beck and Wang (*15*) with slight modifications (*20*). The purified enzymes were stored at −70 °C and showed no loss of activity for 4 months.

Side-Directed Mutagenesis. Oligonucleotide primers were designed to generate mutant T47K of the *T. foetus* HGXPRTase. Plasmid DNA from pBTfprt/DH5α was isolated and used as template for the mutagenesis, using the kit from Stratagene. Following the polymerase chain reaction (PCR), mutant DNA was ligated into pBTfprt and transformed into *E. coli* SØ606 (*16*). Plasmid DNA of the transformants were sequenced for verification, and the recombinant mutant protein was then purified using a similar procedure as for the wild-type.

Enzyme Assay. Kinetic data were collected using a Beckman DU-7 spectrophotometer, equipped with a kinetics accessory. The formation of IMP and GMP were followed spectrophotometrically at 245 and 257.5 nm, respectively (*21*). The formation of XMP was followed spectrophotometrically at 247 nm, which is the wavelength where the difference in absorbance between XMP and xanthine is the largest. All measurements were carried out in 100 mM Tris-HCl, pH 7.0, and 12 mM $MgCl_2$ at 37 °C. Under these conditions, the changes in extinction coefficients for the formation of IMP from hypoxanthine, GMP from guanine, and XMP from xanthine were 1770, 6000, and 5660 M^{-1} cm^{-1}, respectively. The final volume of the assay mixture, containing various amounts of substrates, was 0.5 mL.

IMP pyrophosphorolysis was monitored spectrophotometrically as described by Giacomello and Salerno (*17*) and Yuan et al. (*12*). The formation of hypoxanthine was monitored indirectly by the continuous spectrophotometric assay of uric acid production in the presence of 0.02 unit/mL of xanthine oxidase. The reaction was initiated by the addition of the purified HGXPRTase, and the formation of uric acid was monitored at 293 nm. A molar extinction coefficient of 12 000 M^{-1} cm^{-1} was used for uric acid at this wavelength (*22*). XMP pyrophosphorolysis was also followed by the continuous spectrophotometric assay of uric acid formation from xanthine in the presence of same level of xanthine oxidase. The formation of guanine from GMP was determined by observing uric acid formation in the presence of both guanase (0.01 U/mL) and xanthine oxidase (0.02 U/mL). Again, all measurements were carried out in 100 mM Tris-HCl, pH 7.0, and 12 mM $MgCl_2$ at 37 °C. In these pyrophosphorolysis reactions, the genuine nulceotide substrates are in the form of Mg^{2+} complex as observed in the enzyme-GMP crystal structure data (*19*). From the Data for Biochemical Research, the association constant K_A for MgGMP is about 63 M^{-1}, which would give only 40% of MgGMP at 12 mM Mg^{2+}. For the sake of convenience, only the total concentrations of purine bases, purine nucleotides, PRPP, and PPi are presented in the current report instead of assigning particular complexes. Data were averaged from three different determinations.

Data Analysis. Initial rate data were fitted to eqs 1−5 using kinetics software from BioMetallics, Inc. (k·cat) and IntelliKinetics (KinetAsyst) with Gauss−Newton analysis. The kinetic constants were obtained using weighted linear regression.

For sequential mechanism,

$$v = V_{max}AB/K_{ia}K_b + K_aB + K_bA + AB \quad (1)$$

For equilibrium ordered,

$$v = V_{max}AB/K_aK_b + K_bA + AB \quad (2)$$

For competitive inhibition,

$$v = V_{max}S/[K_m(1 + I/K_{is}) + S] \quad (3)$$

For noncompetitive inhibition,

$$v = V_{max}S/[K_m(1 + I/K_{is}) + S(1 + I/K_{ii})] \quad (4)$$

For uncompetitive inhibition,

$$v = V_{max}S/[K_m + S(1 + I/K_{ii})] \quad (5)$$

The best fits were determined by the relative fit error and errors in the constants. The nomenclature is that of Cleland (*23*): v, initial velocity; V_{max}, maximum velocity; *A*, concentration of substrate A; *B*, concentration of substrate B; K_a, K_m, for A; K_b, K_m, for B; *S* , substrate concentration; K_m, apparent Michaelis constant; K_{is} and K_{ii}, slope and intercept inhibition constants, respectively; *I*, inhibitor concentration.

RESULTS AND DISCUSSION

The steady-state kinetics of synthesis and pyrophosphorolysis of IMP, GMP, and XMP and the product inhibitions of these reactions were analyzed to determine the order of substrate binding and product release. Initial rates of these reactions were proportional to the enzyme concentrations, and substrate inhibition was not observed under these conditions (data not shown).

Steady-State Kinetics. Double-reciprocal plots of initial reaction velocities versus the concentrations of one substrate at a series of fixed concentrations of the other were analyzed for both forward and reverse reactions catalyzed by *T. foetus* HGXPRTase. A family of intersecting lines, with the points of intersections occurring above the 1/[S] axis in most of the plots, indicates a sequential mechanism of addition of substrates and release of products. The data were fitted into the eqs 1 and 2 in Materials and Methods, which descibe a sequential and a equilibrium ordered mechanism, respectively, and was found to fit best to eq 2 describing a equilibrium ordered addition of substrates. Using the method of Ainsworth (*24*), the Michaelis constants K_m and V_{max} for the substrates and products were calculated from secondary plots of the initial velocity experiments and are listed in Table 1. The results indicate that the *T. foetus* HGXPRTase favors hypoxanthine and guanine over xanthine, as indicated by the K_m values for hypoxanthine, guanine, and xanthine, estimated at 3.05 ± 0.54 μM, 2.40 ± 0.74 μM, and 6.08 ± 0.81 μM, respectively. The K_m for xanthine is the lowest among all the XPRTases identified thus far, as compared to 17.6 μM for *Toxoplasma gondii* HGXPRTase (*25*) and 29 μM for *Plasmodium falciparum* HGXPRTase (*26*). The k_{cat}/K_m ratios are 2.92, 1.03, and 0.79 μM^{-1}, s^{-1} for hypoxanthine, guanine, and xanthine, respectively. Thus, while the K_m for xanthine appears to be slightly higher as compared to guanine and hypoxanthine, the catalytic efficiencies for guanine and xanthine are quite similar, whereas hypoxanthine appears to be the best substrate judging from the k_{cat}/K_m values. Hypoxanthine is the only purine base without a substituent at the C-2 position. As observed previously by Somoza et al (*19*), some of the differences in the vicinity of the C-2 position of the bound GMP in the active sites between human HGPRTase and *T. foetus* HGXPRTase may explain why xanthine is a decent substrate for the latter but not at all for the human enzyme. The GMP binding is partly stabilized by hydrophobic interactions between the purine base and the Ile-104 in *T. foetus* HGXPRTase and the Ile-135 in human HGPRTase. In addition, an aromatic side chain that stacks on top of the purine base turns out to be Tyr-156 in the parasite enzyme but Phe-186 in the human enzyme. The phenolic side chain of tyrosine can act as both a hydrogen bond donor as well as an acceptor. Thus, Tyr-156 of the *T. foetus* enzyme could potentially form hydrogen bond with either the N2 of guanine or the O2 of xanthine. This difference in the microenvironment of the base recognition sites of *T. foetus* HGXPRTase and human HGPRTase could be the key structural element on which structure-based design of specific inhibitors could be based.

The values for the K_m of PPi for the schistosomal and human enzymes are of the same order of magnitude as their K_m values for PRPP, both in the 30−40 μM range (*12*, *17*). However, the values of K_m for PPi in the *T. foetus* HGXPRTase-catalyzed reactions (282.91 μM, 165.5 μM, and 739.13 μM for IMP, GMP, and XMP, respectively) are at least 4−16-fold higher than the corresponding K_m values for PRPP (39.9 μM, 46 μM, and 43.77 μM). Thus, it appears that PPi does not bind as well to the *T. foetus* enzyme as compared to the human enzyme. A simple explanation would be that *T. foetus* HGXPRTase catalyzes primarily the forward reaction in fulfilling its biological function of salvaging purines. PPi is known to serve as a source of high energy, partly replacing the function of ATP in *T. foetus* (*27*, *28*). Thus, the weak binding of PPi to HGXPRTase would avail itself for reactions that are coupled to the consumption of a high-energy compound, such as the glycolytic reaction, mediated by a PPi-dependent phosphofructokinase with an estimated K_m value of only 14 μM for PPi (*27*). The intracellular concentration of inorganic pyrophosphate in a closely related organism, *Entamoeba histolytica*, is approximately 0.2 mM (*29*). Although the level of PPi in *T. foetus* is not yet known, it would not be very dissimilar considering the relatedness of the two species and common energetic pathways (*27*). Such a relatively high intracellular concentration of PPi would make the HGXPRTase-catalyzed pyrophosphorolysis possible based on the K_m value alone. However, the poor catalytic effeciency (k_{cat}/K_m) for PPi (0.54 mM^{-1} s^{-1} for HPRTase activity) should prevent the latter from reversing the purine nucleotide synthesis.

Product Inhibition. To identify further, whether the sequential mechanism of *T. foetus* HGXPRTase-catalyzed reaction is ordered or random, product inhibition was analyzed for both the phosphoribosyltransferase and the pyrophosphorolysis reactions (Table 2). PPi was noncompetitive with respect to both guanine and PRPP, while the other products IMP, GMP, and XMP were each found noncompetitive with respect to the corresponding purine bases but competitive with PRPP. In the reverse reaction, PRPP was identified to be noncompetitive to PPi but a competitive inhibitor to IMP, GMP, and XMP. Thus, overall, the results from product inhibition studies of the pyrophosphorolysis reaction agree with those from the phosphoribosyltranferase reaction. PRPP is competitive with respect to the purine nucleotides, but noncompetitive with PPi, whereas the purine nucleotides are competitive with PRPP but noncompetitive with the purine bases. PPi is noncompetitive with both PRPP and the purine bases.

The results from the product inhibition studies of the *T. foetus* HGXPRTase-catalyzed reactions indicate that the purine nucleotides are competitive with respect to PRPP, and when the reaction is reversed, PRPP is competitive with respect to the Mg-complexed purine nucleotides. All other

Table 2: Product Inhibition of Both Forward and Reverse Reactions of HGXPRTase

inhibitor	substrate	pattern type	K_{ii} (μM)	K_{is} (μM)
IMP	hypoxanthine	noncompetitive	74.5 ± 5.2	6.8 ± 0.11
PPi	hypoxanthine	noncompetitive	168 ± 6.1	197 ± 11.4
IMP	PRPP	competitive		8.3 ± 0.41
PPi	PRPP	noncompetitive	155 ± 40.4	980 ± 181
PRPP	PPi	noncompetitive	29.5 ± 2.8	82 ± 4.5
PRPP	IMP	competitive		109 ± 20.7
GMP	guanine	noncompetitive	22 ± 2.2	20 ± 2.8
PPi	guanine	noncompetitive	345 ± 28.5	410 ± 88.9
GMP	PRPP	competitive		14 ± 1.9
PPi	PRPP	noncompetitive	690 ± 110	280 ± 44.8
PRPP	PPi	noncompetitive	280 ± 34.7	65 ± 15.6
PRPP	GMP	competitive		28 ± 5.4
XMP	xanthine	noncompetitve	42.87 ± 1.67	59.56 ± 5.54
PPi	xanthine	noncompetitive	7310 ± 430	5904 ± 1690
XMP	PRPP	competitive		7.18 ± 0.08
PPi	PRPP	noncompetitive	4985 ± 330	3725 ± 220
PRPP	PPi	noncompetitive	472.21 ± 23.9	590.82 ± 34.6
PRPP	XMP	competitive		210.04 ± 14.1

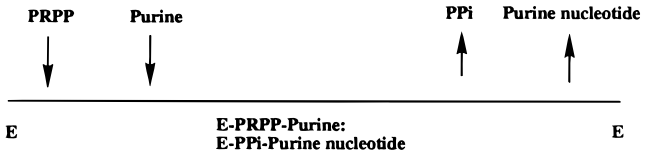

FIGURE 1: Ordered bi−bi mechanism of the *T. foetus* HGXPRTase-catalyzed reactions.

product inhibition patterns were noncompetitive. Thus, PRPP and the Mg-complexed purine nucleotides apparently bind to the same enzyme form, which has to be the free enzyme. Consequently, the minimum kinetic model that describes the experimental data must be an ordered bi−bi mechanism. PRPP must bind to the enzyme first and the Mg-complexed purine nucleotides must be released last. Figure 1 shows the proposed mechanism for the *T. foetus* HGXPRTase-catalyzed reaction.

The product inhibition studies of a few other PRTases have indicated that both the yeast and *S. mansoni* HGPRTases appear to follow an ordered bi−bi mechanism identical to that described in Figure 1 (*12*, *30*). Flow dialysis experiments of the yeast HGPRTase identified the enzyme−PRPP complex, but no enzyme complex with the purine bases were detected (*30*) which support the same ordered bi−bi model. The human HGPRTase (*11*) has also been shown recently to have a similar mechanism of ordered substrate binding and product release. These enzymes thus belong to the same family of phosphoribosyltransferases with the same mechanism of catalysis.

The Role of Threonine 47 in T. foetus HGXPRTase. One of the most interesting findings in the present investigations is probably the identification of an unusually high K_m for PPi. The X-ray crystallographic data on the structure of *T. foetus* HGXPRTase (*19*) have suggested that threonine-47 in the enzyme protein corresponds to lysine-68 in human HGPRTase which is located in the loop between β-strand 3 and α-helix 3 and has been proposed by Eads *et al.* (*18*) to perform the function of binding to PPi, presumably largely through ionic interactions. This hypothesis is supported by the crystal structure of OPRTase/PRPP−orotate complex (*31*) where there is a lysine-73 at an equivalent position, and it is positioned to form a hydrogen bond with the β-phosphate oxygen of the PPi moiety in PRPP. This lysine residue is well conserved among most of the HGXPRTases except for *T. foetus* HGXPRTase (*16*) and *Giardia lamblia* guanine phosphoribosyltransferase (GPRTase) (*32*) where the lysine is replaced by threonine in both cases. Threonine-47 in *T. foetus* HGXPRTase is located in a similar loop between β-strand 2 and α-helix 2 (*19*). The loop is a prominent structure of the active-site clefts of both the human and *T. foetus* enzymes. The amino acid residues (residues 67−70 in human and 46−49 in parasite enzyme) forming this loop [LK(T)GG(S)] are highly conserved across the family of purine phosphoribosyltransferases. Interestingly, the loop in *T. foetus* HGXPRTase contains a cis peptide between Leu-46 and Thr-47 (*19*); which appears to be quite conserved among the *S. mansoni* HGPRTase (Focia, P. J., personal communication), *E. coli* XPRTase (*33*), and *E. coli* OPRTase (*34*). A recent article on the structure of glutamine phosphoribosylpyrophosphate amidotransferase (*35*) has also shown the presence of a *cis*-peptide, binding to the pyrophosphate group of Mn^{2+}-cPRPP via the peptide NH. The conformation of the peptide between Leu-67 and Lys-68 in human HGPRTase was not well resolved thus far (*18*). This *cis*-peptide conformation could influence the formation of hairpin turn at this point and the orientation of the residues of the loop in the protein. A comparison of the structures of the *T. foetus* and the human enzyme (Figure 2) suggests that the loop in *T. foetus* HGXPRTase is further away from the active site when compared with that in the human HGPRTase. This lengthened distance, coupled with the apparent inability of Thr-47 in forming ionic bond with PPi, could have contributed to the high K_m values for PPi in *T. foetus* HGXPRTase-catalyzed reactions.

To verify this hypothesis, we used site-directed mutagenesis to obtain the single amino acid mutant of the *T. foetus* HGXPRTase, which had threonine 47 replaced by lysine. This T47K mutant was purified to apparent homogeneity using a similar procedure as for the wild-type (*16*) (Figure 3). The K_m value for PPi in the mutant enzyme-catalyzed reaction was determined and compared with that from the wild-type enzyme. Figure 4 represents the kinetic data from the two enzyme-catalyzed reactions with PPi as the varying substrate at different fixed concentrations of XMP. The K_ms for PPi in the wild-type enzyme catalayzed reactions range

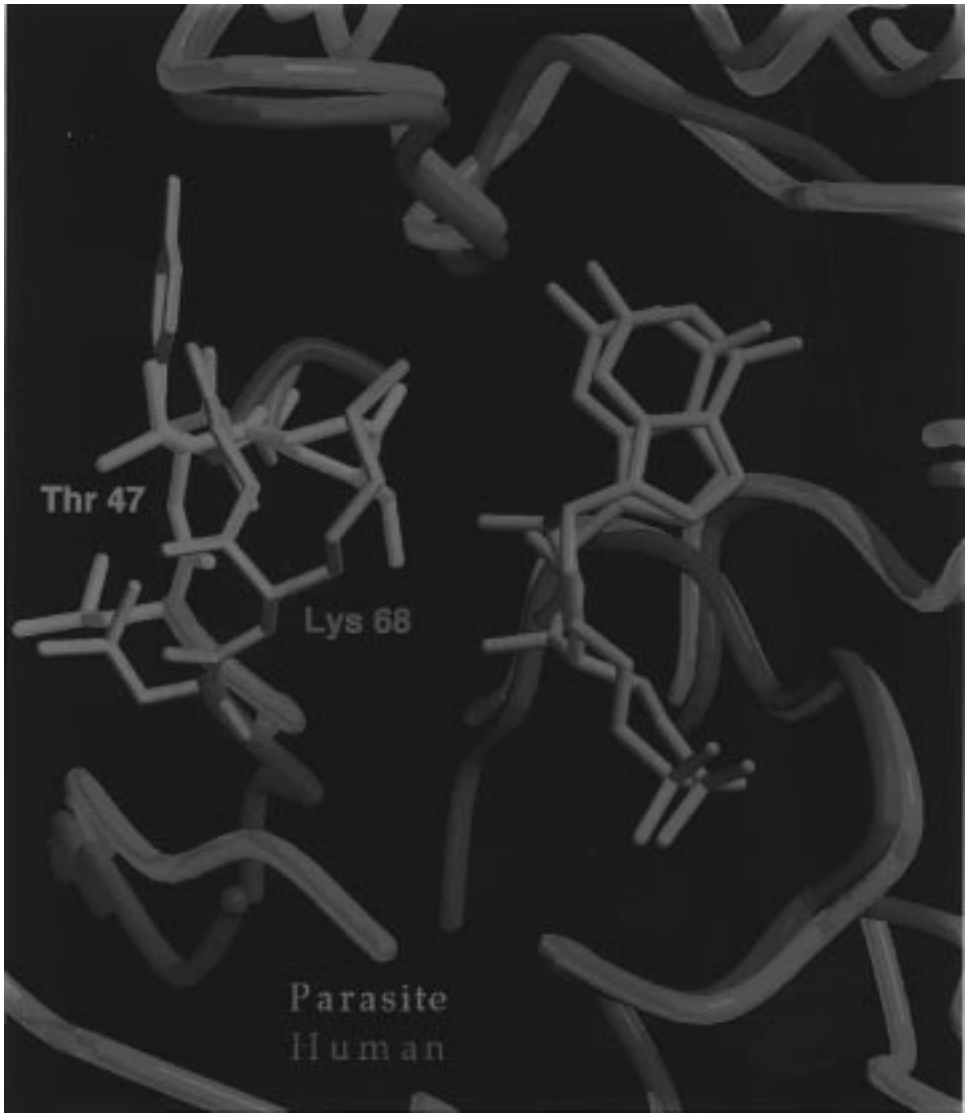

FIGURE 2: Comparison of the active sites of the *T. foetus* HGXPRTase (green) (*19*) and the human HGPRTase (blue) (*18*), based on a superposition of the two molecules of GMP.

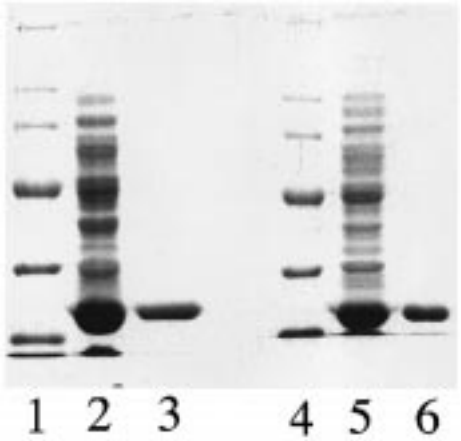

FIGURE 3: SDS−PAGE analysis of the *T. foetus* wild-type and T47K mutant HGXPRTase expressed in transformed *E. coli*. Lane 1, low-range molecular mass protein marker (14−66 kDa); 2, crude lysate of *E. coli* SØ606 expressing wild-type HGXPRTase; 3, purified wild-type HGXPRTase; 4, Low-range molecular mass protein marker (14−66 kDa); 5, crude lysate of *E. coli* SØ606 expressing the T47K mutant; 6, purified T47K mutant.

from 165.5 to 739.13 μM (see Table 1), whereas those in the mutant enzyme-catalyzed reactions range from 72.29 to 96.25 μM (see Table 3). These dramatic decreases in the K_m values for PPi in the mutant enzyme-catalyzed reactions range from 4−10-fold. They render a strong support to the belief that Thr-47 is involved in binding to PPi and that the lack of ionic interaction between the two is responsible, at least partly, for the high K_m for PPi in the wild-type *T. foetus* HGXPRTase-catalyzed reaction. The k_{cat} values of the T47K mutant enzyme-catalyzed reactions, however, change very little from the wild-type, which suggest that the release of PPi from the enzyme and the binding of PPi to the enzyme do not constitute the rate-limiting step in the reactions of both directions regardless of the K_m value for PPi. The K_m values for hypoxanthine and IMP in the T47K mutant-catalyzed reactions showed no appreciable difference from the wild-type (Table 3), suggesting a lack of involvement of residue 47 in binding the purine bases or nucleotides. The K_m value for PRPP in the T47K mutant-catalyzed forward reaction showed also no significant change from the wild-type enzyme (Table 3). This lack of difference suggests that the loop of residues 46−49 in the parasite enzyme is not involved in PRPP binding, which could be attributed to its further removed position from the active site (*19*). However, since Thr-47 does appear to bind to PPi, a swing of the loop

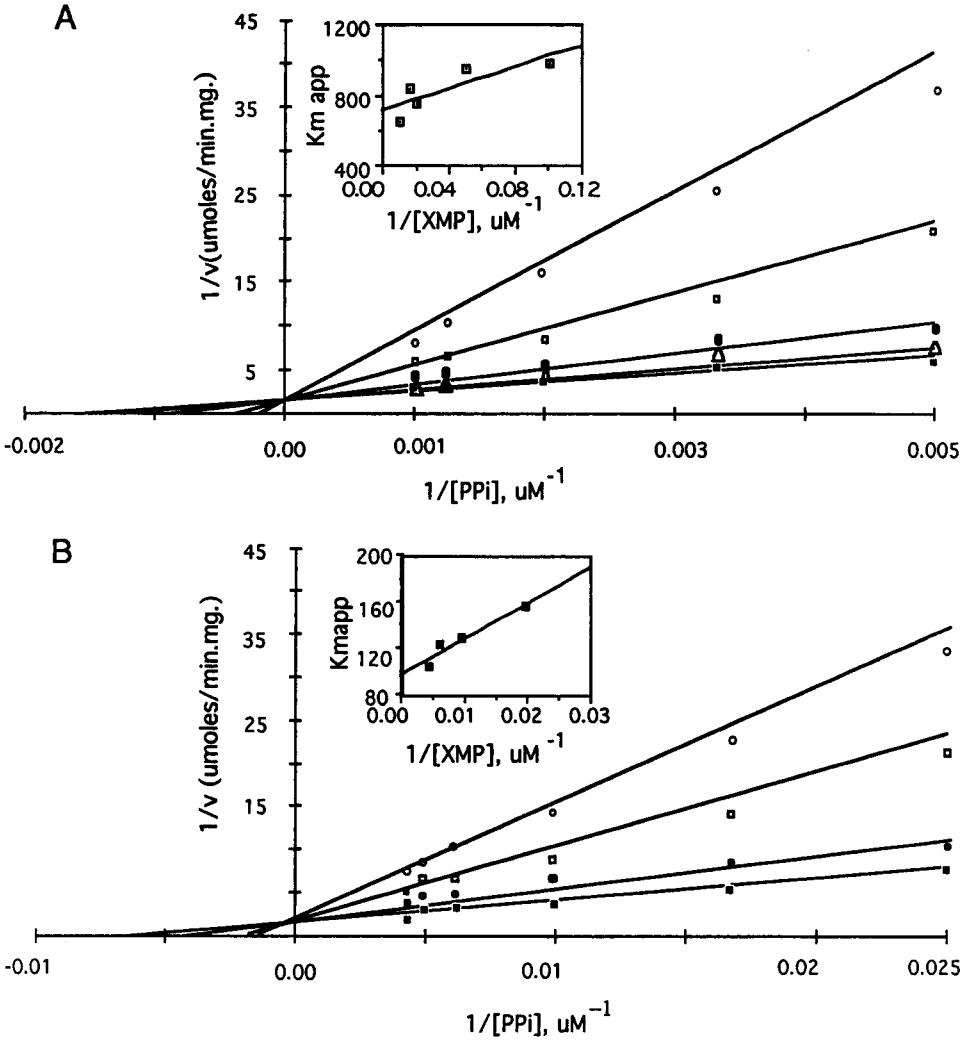

FIGURE 4: Initial velocity patterns for *T. foetus* HGXPRTase-catalyzed reverse reactions with PPi as the variable substrate at different concentrations of XMP. All other conditions were as described in the Materials and Methods. (Inset) Replot of K_m^{app} with respect to the reciprocal micromolar concentrations of XMP. A, wild-type *T. foetus* HGXPRTase; B, *T. foetus* HGXPRTase T47K mutant.

Table 3: Kinetic Constants of the *T. foetus* HGXPRTase T47K Mutant-Catalyzed Reactions

substrate	K_m (μM)	V_{max} (μmol min^{-1} mg^{-1})	k_{cat} (s^{-1})
	HPRTase		
PRPP	32.13 ± 3.6	15.34 ± 1.94	5.49 ± 0.7
PPi	79.66 ± 11.9	0.2 ± 0.02	0.07 ± 0.1
Hypoxanthine	3.39 ± 0.24	19.48 ± 1.27	6.71 ± 0.44
IMP	13.27 ± 2.1	0.37 ± 0.03	0.12 ± 0.01
	GPRTase		
PRPP	39.5 ± 4.2	3.77 ± 0.17	1.3 ± 0.06
PPi	72.49 ± 2.9	1.09 ± 0.22	0.38 ± 0.08
	XPRTase		
PRPP	28.37 ± 3.2	2.64 ± 0.2	0.91 ± 0.07
PPi	96.25 ± 6.7	0.26 ± 0.03	0.09 ± 0.01

toward the active site may occur during the phosphoribosyltransferase reaction to make this possible. This conclusion strongly supports the hypothesis that movement and conformational change of this loop may occur during the catalysis of human (*11*) and schistosomal HGPRTase (Focia, P. J., personal communication). It is not known at present, however, whether the *cis*-peptide conformation of the loop remains unchanged in the T47K mutant, which must wait for the X-ray crystallographic analysis in the future.

ACKNOWLEDGMENT

We thank Dr. John Somoza for critical review of the manuscipt and for providing Figure 2. We also thank Dr. Solomon Mpoke for making the T47K mutant.

REFERENCES

1. Musick, W. D. L. (1981) *CRC Crit. Rev. Biochem. 11*, 1−34.
2. Berens, R. L., Marr, J. J., LaFon, S. W., and Nelson, D. J. (1981) *Mol. Biochem. Parasitol. 3*, 187−196.
3. Fish, W. R., Marr, J. J., and Berens, R. L. (1982) *Biochim. Biophys. Acta 714*, 422−428.
4. Krug, E. C., Marr, J. J., and Berens, R. L. (1989) *J. Biol. Chem. 264*, 10601−10607.
5. Marr, J. J., Berens, R. L., and Nelson, D. J. (1978) *Biochim. Biophys. Acta 44*, 360−371.
6. Schwartzman, J. D., and Pfefferkorn, E. R. (1982) *Exp. Parasitol. 53*, 77−86.
7. Walsh, C. J., and Sherman, I. W. (1968) *J. Protozool. 15*, 763−770.
8. Wang, C. C., and Aldritt, S. L. (1983) *J. Exp. Med. 158*, 1703−1712.
9. Wang, C. C., and Simashkevich, P. M. (1981) *Proc. Natl. Acad. Sci. U.S.A. 78*, 6618−6622.
10. Wang, C. C., Verham, R., Rice, A., and Tzeng, S. (1983) *Mol. Biochem. Parasitol.* **8**, 325−337.

11. Xu, Y., Eads, J., Sacchettini, J. C., and Grubmeyer, C. (1997) *Biochemistry 36*, 3700−3712.
12. Yuan, L., Craig, S. P., III, McKerrow, J. H., and Wang, C. C. (1992) *Biochemistry 31*, 806−810.
13. Fitzgerald, P. R. (1986) *Vet. Clinic No. Am.: Food Animal Practice 2*, 277−282.
14. Parsonson, I. M., Clark, B. L., and Dufty, J. (1974) *Aust. Vet. J. 50*, 421−423.
15. Beck, J. T., and Wang, C. C. (1993) *Mol. Biochem. Parasitol. 60*, 187−194.
16. Chin, M. S., and Wang, C. C. (1994) *Mol. Biochem. Parasitol. 63*, 221−229.
17. Giacomello, A., and Salerno, C. (1978) *J. Biol. Chem. 253*, 6038−6044.
18. Eads, J. C., Scapin, G., Xu, Y., Grubmeyer, C., and Sacchettini, J. C. (1994) *Cell 78*, 325−334.
19. Somoza, J. R., Chin, M. S., Focia, P. M., Wang, C. C., and Fletterick, R. J. (1996) *Biochemistry 35*, 7032−7040.
20. Kanaani, J., Somoza, J. R., Maltby, D.. and Wang, C. C. (1996) *Eur. J. Biochem. 239*, 764−772.
21. Hill, D. L. (1970) *Biochem. Pharmacol. 19*, 545−557.
22. Kalckar, H. M. (1947) *J. Biol. Chem. 167*, 429−443.
23. Cleland, W. W. (1963) *Biochim. Biophys. Acta 67*, 104−137.
24. Ainsworth, S. (1977) in *Steady-state enzyme kinetics*, University Park Press, Baltimore, Maryland.
25. Donald, R. G. K., Carter, D., Ullman, B., and Roos, D. S. (1996) *J. Biol. Chem. 271*, 14010−14019.
26. Queen, S. A., Jagt, D. V., and Reyes, P. (1988) *Mol. Biochem. Parasitol. 30*, 123−134.
27. Mertens, E. (1991) *Fed. Eur. Biochem. Soc. Lett. 285*, 1−5.
28. Müller, M. (1992) *BioSystems 28*, 33−40.
29. Saavedra-Lira, E., and Perez-Montfort, R. (1996) *Arch. Med. Res. 27*, 257−264.
30. Ali, L. Z., and Sloan, D. L. (1982) *J. Biol. Chem. 257*, 1149−1155.
31. Scapin, G., Grubmeyer, C., and Sacchettini, J. C. (1994) *Biochemistry 33*, 1287−1294.
32. Sommer, J. M., Ma, H., and Wang, C. C. (1996) *Mol. Biochem. Parasitol. 78*, 185−193.
33. Vos, S., de Jersey, J., and Martin, J. L. (1997) *Biochemistry 36*, 4125−4134.
34. Henriksen, A., Aghajari, N., Jensen, K. F., and Gajhede, M. (1996) *Biochemistry 35*, 3803−3809.
35. Krahn, J. M., Kim, J. H., Burns, M. R., Parry, R. J., Zalkin, H., and Smith, J. L. (1997) *Biochemistry 36*, 11061−11068.

BI972515H